Interpretation of the LHCb $P_c(4312)^+$ Signal

C. Fernández-Ramírez,[1,*] A. Pilloni,[2,3,†] M. Albaladejo,[4] A. Jackura,[5,6]
V. Mathieu,[4] M. Mikhasenko,[7] J. A. Silva-Castro,[1] and A. P. Szczepaniak[4,5,6]
(Joint Physics Analysis Center)

[1] *Instituto de Ciencias Nucleares, Universidad Nacional Autónoma de México, Ciudad de México 04510, Mexico*
[2] *European Centre for Theoretical Studies in Nuclear Physics and Related Areas (ECT*) and Fondazione Bruno Kessler, I-38123 Villazzano (TN), Italy*
[3] *INFN Sezione di Genova, Genova, I-16146, Italy*
[4] *Thomas Jefferson National Accelerator Facility, Newport News, VA 23606, USA*
[5] *Center for Exploration of Energy and Matter, Indiana University, Bloomington, IN 47403, USA*
[6] *Physics Department, Indiana University, Bloomington, IN 47405, USA*
[7] *CERN, 1211 Geneva 23, Switzerland*

We study the nature of the new signal reported by LHCb in the $J/\psi\, p$ spectrum. Based on the S-matrix principles, we perform a minimum-bias analysis of the underlying reaction amplitude, focusing on the analytic properties that can be related to the microscopic origin of the $P_c(4312)^+$ peak. By exploring several amplitude parameterizations, we find evidence for the attractive effect of the $\Sigma_c^+\bar{D}^0$ channel, that is not strong enough, however, to form a bound state.

Introduction.— From first principles of QCD, it is still unknown why the vast majority of hadrons appear to follow the valence quark model pattern proposed by Gell-Mann and Zweig [1, 2]. The discovery of genuine multiquark states would be a major milestone in the history of strong interactions. In recent years, several exotic candidates have been reported [3–8]. The observation by LHCb of a narrow peak at 4312 MeV in the $J/\psi\, p$ invariant mass distribution in the $\Lambda_b^0 \to J/\psi\, p\, K^-$ decay [9] points to yet another hidden charm pentaquark. A hint of this signal, labeled $P_c(4312)^+$, was already visible in the earlier LHCb analyses, but it was statistically insignificant [10, 11]. The fact that such a narrow (~ 10 MeV) peak stands out in what otherwise appears to be a smooth background permits a simple one-dimensional analysis, although determination of its quantum numbers will require the full 6-dimensional amplitude analysis fitting both the energy and angular dependencies.

Remarkably, the signal peaks 2 MeV below the $\Sigma_c^+\bar{D}^0$ threshold. It is often said that an enhancement in the proximity of a two-particle threshold is a manifestation of a hadron molecule composed of the two particles. A $J^P = 1/2^-$ $\Sigma_c^+\bar{D}^0$ molecule in the 4260-4300 MeV region was indeed predicted in various models [12–17]. However, this is not the only possibility. Virtual states can be produced as well [18], for example by an attractive interaction that is not strong enough to bind a state, as in neutron-neutron scattering [19]. Genuine compact pentaquark interpretations are also possible. A $3/2^-$ pentaquark was found in [20] at 4329 MeV. Compact diquark-diquark-antiquark states with spin assignment $(1/2, 3/2)^-$ at ~ 4260 MeV, together with orbital excitations $(1/2, 3/2)^+$ at ~ 4330 MeV, were predicted in [21], and are compatible with a $P_c(4312)^+$.[1]

These various interpretations of the $P_c(4312)^+$ signal are related to different analytic properties of the $\Lambda_b^0 \to J/\psi\, p\, K^-$ amplitude. In this Letter we investigate what can be concluded from the LHCb data on the $J/\psi\, p$ mass spectrum as far as the nature of the $P_c(4312)^+$ peak is concerned.

Data and analysis of the $P_c(4312)^+$ region.— It is a common practice to interpret peaks by postulating a theoretical model and comparing it to data (see for example [24–33]). In contrast, we follow here a minimally biased approach. We construct a reaction amplitude that respects the generic principles of the S-matrix theory. The S-matrix principles of unitarity and analyticity cannot fully determine the partial wave amplitudes, and unless the complete (infinite-dimensional, crossing symmetric) S-matrix is calculated, there will be undetermined parameters. These encode specifics of the underlying QCD dynamics. We leave them to be determined by data, rather than by a given model. We fit the $\cos\theta_{P_c}$-weighted spectrum $dN/d\sqrt{s}$ measured in [9], with $\sqrt{s}$ being the $J/\psi\, p$ invariant mass, and restrict the analysis to the 4250-4380 MeV region where the $P_c(4312)^+$ is found. As a crosscheck we also analyze the unweighted $J/\psi\, p$ spectrum in the same region, both with and without the $m_{Kp} > 1.9$ GeV cut.

As mentioned, the effect of the $\Sigma_c^+\bar{D}^0$ threshold looks prominent in data. We thus consider an amplitude which

[1] We recall that the compact pentaquark predictions rely on the preferred determination of the quantum numbers of the $P_c(4380)^+$ and $P_c(4450)^+$, which might change when the two-state structure of the latter peak will be taken into account. The role of thresholds in multiquark states has been discussed in [22, 23].

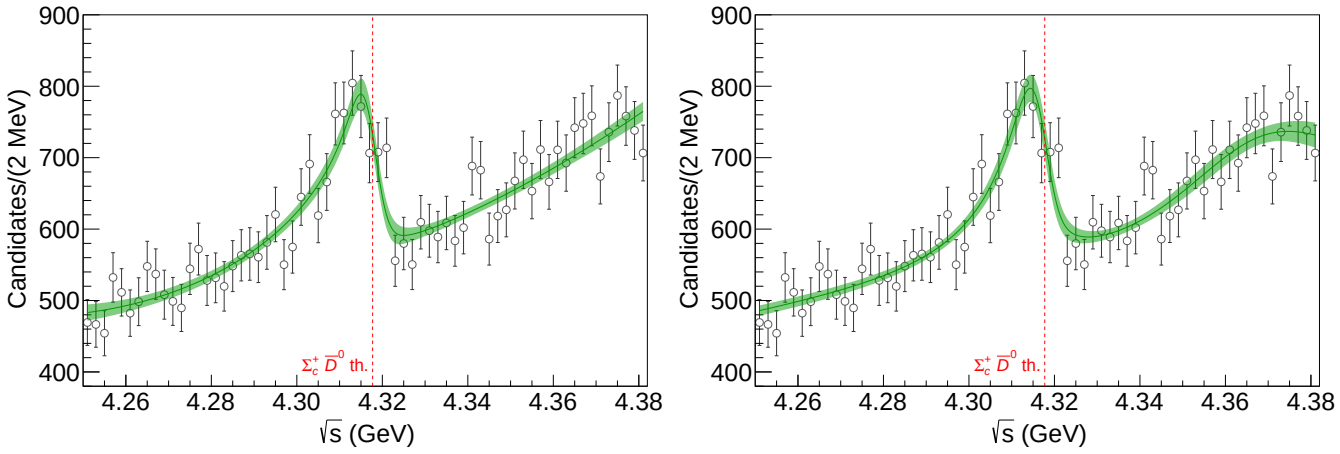

FIG. 1. Fits to the $\cos\theta_{P_c}$-weighted $J/\psi p$ mass distribution from LHCb [9] according to cases A (left) and B (right). The amplitude of case A is expressed in the scattering length approximation, *i.e.* $c_{ij} = 0$ in Eq. (3), and is able to describe either bound (molecular) or virtual states. The amplitude of case B is given in the effective range approximation, *i.e.* finite c_{ii}, and extends the description to genuine pentaquark states. The solid line and green band show the result of the fit and the 1σ confidence level provided by the bootstrap analysis, respectively.

couples $J/\psi p$ (channel 1) and $\Sigma_c^+ \bar{D}^0$ (channel 2). There is another nearby threshold, 6 MeV above, which corresponds to the opening of the isospin partner, $\Sigma_c^{++} D^-$ state. The $J/\psi p$ spectrum suggests this heavier threshold to be less important. We thus discuss the two-channel case first, where the analytic properties are more transparent. We comment on the results of three-channel fit further below. The events distribution is given by

$$\frac{dN}{d\sqrt{s}} = \rho(s)\left[|F(s)|^2 + B(s)\right], \tag{1}$$

where $\rho(s)$ is the phase space factor. We assume that the $P_c(4312)^+$ signal has well defined spin, *i.e.* it appears in a single partial wave $F(s)$. The background $B(s)$ from all other partial waves is added incoherently, and parameterized with a linear polynomial. The amplitude $F(s)$ is a product of a function $P_1(s)$ which provides the production of $J/\psi p K^-$,[2] and the $T_{11}(s)$ amplitude, which describes the $J/\psi p \to J/\psi p$ scattering,

$$F(s) = P_1(s)\, T_{11}(s), \quad \left(T^{-1}\right)_{ij} = M_{ij} - i k_i\, \delta_{ij}, \tag{2}$$

with $i, j = 1, 2$. Here $k_i = \sqrt{s - s_i}$ with $s_1 = (m_\psi + m_p)^2$, $s_2 = (m_{\Sigma_c^+} + m_{\bar{D}^0})^2$ are the thresholds of the two channels. In principle, one could also add the off-diagonal $P_2(s)T_{21}(s)$ term. This would not change the analytic properties, and would provide a nonzero value of $F(s)$ when $T_{11}(s)$ vanishes. The presence of a zero would be a relevant feature if no background were present, and in that case $P_2(s)T_{21}(s)$ might be needed. In our case, we suppress such a term to reduce the number of free parameters. For the real symmetric 2×2 matrix $M(s)$ we use the first-order effective range expansion

$$M_{ij}(s) = m_{ij} - c_{ij} s, \tag{3}$$

which is sufficient when considering the possibility of at most a single threshold state (virtual or molecular) and a compact state [34]. In the single channel case, this parameterization has often been discussed in the context of the Weinberg compositeness criterion [32, 35–39]. The function $P_1(s)$ is analytic in the data region, and, given the small mass range considered, it can be parameterized with a first order polynomial. For particle masses, we use the PDG values $m_{\Sigma_c^+} = 2452.9\,\text{MeV}$ and $m_{\bar{D}^0} = 1864.83\,\text{MeV}$ [40]. Since the width of the Σ_c^+ is similar to the experimental resolution we neglect its effect. More details about the parameterizations and the fit results are in the Supplemental Material [41].

Because of the square roots in k_1 and k_2, the amplitude has branch cuts opening at the two thresholds. Through analytic continuation to complex values of s, one accesses four different Riemann sheets (see also Fig. 2 of [42]). The physical region between the two thresholds is connected to the lower half of the II sheet. Similarly, the physical region above the $\Sigma_c^+ \bar{D}^0$ threshold is connected to the lower half of the III sheet. Poles in these sheets will appear as peaks with Breit-Wigner-like lineshape in data, if they lie below the respective physical regions, *i.e.* between the two thresholds for the II sheet, and above the heavier one for the III. From the II sheet, if one continuously moves to the upper half plane above the higher threshold, one enters the upper half of the IV sheet. Since the latter is hidden from the physical region, a pole here will manifest in data as a cusp at the $\Sigma_c^+ \bar{D}^0$ threshold.

[2] The $P_1(s)$ function absorbs also the cross channel Λ^* resonances projected into the same partial wave as $P_c(4312)^+$.

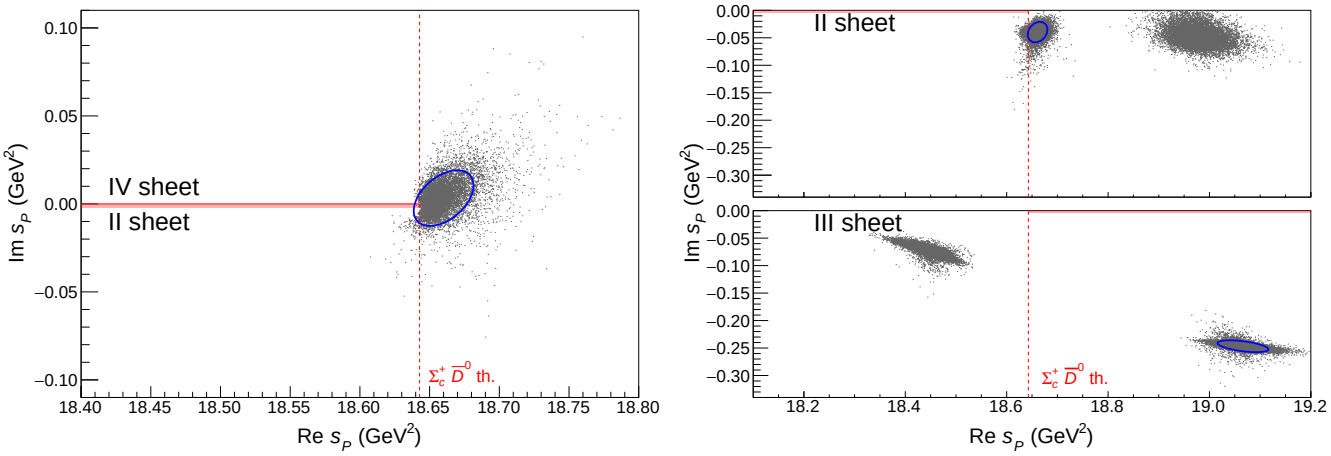

FIG. 2. Poles obtained from the 10^4 bootstrap fits for cases A (left) and B (right). The physical region is highlighted with a pink band. For case A the poles lie on the II and IV Riemann sheets (which are continuously connected above the $\Sigma_c^+\bar{D}^0$ threshold). For each bootstrap fit only one pole appears in this region and the blue ellipse accounts the 68% of the cluster concentrating above threshold. The right plots show the poles for case B. For each bootstrap fit we obtain a pole on the II sheet and its partners on the III sheet. The higher mass pole on the II sheet and its partner on the III are above the fitted energy range and try to capture the bump-like structure that appears at 4370 MeV. The lower mass pole on the II sheet and its partner on the III are responsible for the $P_c(4312)^+$ signal. The blue ellipses account for 68% of the two clusters.

Results and discussion.— In order to determine the sensitivity of data to various scenarios, we consider two cases. In case A, we set $c_{ij} = 0$, which corresponds to the scattering length approximation. This choice is substantially equivalent to the universal amplitude used in [43] to describe the $X(3872)$. It is known that the amplitude $T_{11}(s)$ can have a pole on either the II or IV sheet, but not on the III [34]. This pole is entirely due to the opening of the heavier channel, and therefore it is a measure of the strength of the $\Sigma_c^+\bar{D}^0$ interaction. Further interpretations can be drawn by considering how the pole moves as the coupling between the two channels is turned off. In this case, the pole could either move to the real axis of the physical sheet below the heavier threshold, thus representing a bound molecule, or move onto the real axis of the unphysical sheet, corresponding to an unbound, virtual state. In case B, we let the diagonal effective ranges c_{ii} float. The off-diagonal c_{12} does not add other singularities, is not needed to describe data and we set it to zero. In this case, poles related to the threshold as the ones just discussed are possible but not guaranteed, however other poles can appear on the II and III sheet.[3] The latter can be interpreted as originating from genuine pentaquark particles, with bare masses $\sqrt{m_{ii}/c_{ii}}$, that move into the complex plane and acquire a width when coupled to the open channels. The other clear distinction between these and the threshold-related poles discussed above is that the latter move far less in the complex plane when the channel couplings are varied.

We fit the data using MINUIT [44] and taking into account the experimental resolution reported in [9]. The initialization of the parameters is chosen by randomly generating $O(10^5)$ different sets of values. The amplitude in Eq. (1) is not protected against unphysical poles in the I sheet. Fits with such poles are discarded. The best solutions for the two cases have comparable $\chi^2/\text{dof} \simeq 0.8$. Figure 1 shows both fits to the data. The preference of case B over A is only at 1.8σ level calculated with the Wilks's theorem [45], and we consider both cases as equally acceptable. In both cases, we find a pole 2 MeV above the $\Sigma_c^+\bar{D}^0$ threshold, on the IV sheet for case A and II sheet for case B. For case B, additional poles appear further away from the $\Sigma_c^+\bar{D}^0$ threshold, on the II and III sheet. These do not affect the $P_c(4312)^+$ signal.

To estimate sensitivity of the pole positions to the uncertainties in the data, we use the bootstrap technique [46, 47], *i.e.* we generate 10^4 pseudodata sets and fit each one of them. The statistical fluctuations in data reflect into the the uncertainty band plotted in Fig. 1. Moreover, for each of these fits, we determine the pole positions, as shown in Fig. 2.

In case A, it is possible to identify a cluster of virtual state poles across the II and IV sheet above the $\Sigma_c^+\bar{D}^0$ threshold (see also the discussion in [48]). If we use the customary definition of mass and width, $M_P = \text{Re}\,\sqrt{s_p}$, $\Gamma_P = -2\,\text{Im}\,\sqrt{s_p}$ the main cluster has $M_P = 4319.7 \pm 1.6$ MeV, $\Gamma_P = -0.8 \pm 2.4$ MeV, where positive or negative values of the width correspond to II or IV sheet poles, respectively. To establish the nature of this singularity, we track down the movement of the poles as the coupling between the two channels is reduced. By taking $m_{12} \to 0$,

[3] It is easy to check that case A with $c_{ii} = 0$ has exactly 2 pairs of conjugate poles in the various sheets, while the general case B has exactly 4. Only the closest to the physical region are relevant.

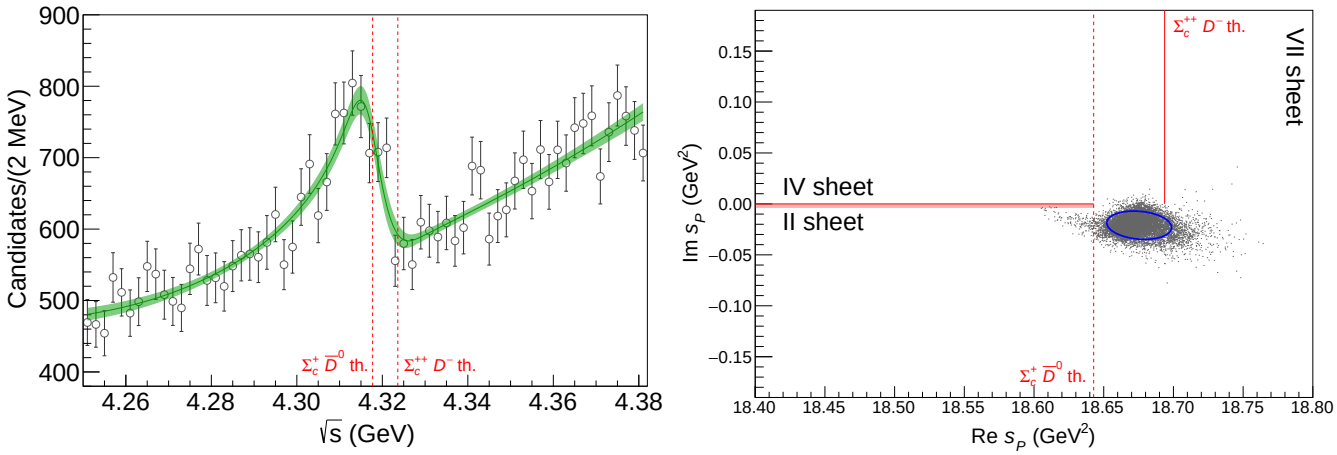

FIG. 3. Fit to the $\cos\theta_{P_c}$-weighted $J/\psi p$ mass distribution (left) and pole positions (right) for the 3-channel case. Notation is the same as in Figs. 1 and 2. The poles are obtained from the 10^4 bootstrap fits and lie on the II and IV Riemann sheets (which are continuously connected above the $\Sigma_c^+\bar{D}^0$ threshold) and on the VII sheet (which is continuously connected to the II above the $\Sigma_c^{++}D^-$ threshold). For each bootstrap fit only one pole appears in this region. The blue ellipse accounts the 68% of the cluster concentrating above the $\Sigma_c^+\bar{D}^0$ threshold.

we can see how the cluster moves over to the upper side of the IV sheet and ends up on the real axis below the $\Sigma_c^+\bar{D}^0$ threshold [41]. The fraction of poles that reach the real axis from the lower side of the II sheet is 0.7% only, and thus not significant. This result reinforces the interpretation of the pole as an unbound virtual state, meaning that the binding between the Σ_c^+ and the $\bar{D}^0$ is insufficient to form a molecule.

In case B, the poles on the II sheet accumulate in two clusters. The one closer to threshold has $M_P = 4319.8 \pm 1.5\,\text{MeV}$ and $\Gamma_P = 9.2 \pm 2.9\,\text{MeV}$, and it is the one responsible for the $P_c(4312)^+$ signal. As we did for case A, we study the motion of the poles as the channels decouple. The lighter cluster migrates onto the IV sheet, where it hits the zero of $T_{11}(s)$, and annihilates when $m_{12} = 0$. Since the pole does not survive the decoupling, it is entirely due to the interaction between the two channels, and its motion to the furthest unphysical sheet also suggest a virtual state nature for the $P_c(4312)^+$ as in case A.

The other poles, which are located further away from the $\Sigma_c^+\bar{D}^0$ threshold can also be interpreted. There are two clusters of poles on the III sheet, one far above the $\Sigma_c^+\bar{D}^0$ threshold, the other below (see Fig.2). The former could correspond to a resonance with standard Breit-Wigner lineshape as it appears to originate from the broad bump in the mass spectrum centered at $\sqrt{s} \sim 4.37\,\text{GeV}$.[4] As $m_{12} \to 0$, the two III sheet clusters move close to each other, and the heavier one disappears, multiplied by the amplitude zeros when $m_{12} = 0$. In this uncoupled limit, only one pole per channel is left. Furthermore, as the channels close, which is achieved by replacing $ik_i \to \lambda ik_i$ and letting $\lambda \to 0$, the poles move onto the real axis. It is worth noting that the fit chooses almost identical values for the ratios $m_{11}/c_{11} \simeq m_{22}/c_{22}$. This ratio determines the independent positions of the bare poles on the real axis in the two uncoupled channels and being equal, suggests existence of a single compact pentaquark. Although the presence of such state is not significant, as clear from the fact that case A fits data equally well, and no conclusion can be drawn before the complete amplitude analysis. It is an interesting speculation that such an enhancement might be related to the broad $P_c(4380)^+$ observed by the previous LHCb analysis [10].

We also performed a study of the three-channel case, including the $\Sigma_c^{++}D^-$ threshold. To simplify the approach we work in the scattering length approximation (as in case A) and in the isospin limit for the fitting parameters. The result of the fit and the pole positions are shown in Fig. 3 and details can be found in the Supplemental Material [41]. We find a single pole close to the $\Sigma_c^+\bar{D}^0$ threshold on the II sheet. No other pole appears close to the physical axis above the $\Sigma_c^{++}D^-$ threshold. When the couplings between the channels are reduced, the pole quickly moves far to the left, and cannot interpreted as a physical state. We therefore conclude that the $P_c(4312)^+$ signal could be a result of a complicated interplay of thresholds and feeble $\Sigma_c\bar{D}$ interactions.

We perform further systematic analyses by considering Flatté and K-matrix parameterizations. Using a single K-matrix pole with an off-diagonal constant background leads to a pole on the II sheet in the same position as case A. On the other hand, the Flatté parameterization

[4] This is seen in both weighted and unweighted datasets. We also note that the $\Sigma_c(2520)\bar{D}^0$ threshold is close at 4383.24 MeV.

does not provide a good description of the $P_c(4312)^+$ peak, and does not generate stable poles in the region of interest.

As a crosscheck we fit all the above approaches to the unweighted $J/\psi\, p$ spectrum in the same region, both with and without the $m_{Kp} > 1.9\,\text{GeV}$ cut. Results are consistent.

Conclusions.— In summary, we have studied the $P_c(4312)^+$ reported by LHCb in the $J/\psi\, p$ spectrum. We considered a reaction amplitude which satisfies the general principles of S-matrix theory, with a minimum bias from the underlying theory. The analytic properties of the amplitudes can be related to the microscopic origin of the signal. We fitted the LHCb mass spectrum in the 4312 GeV mass region including the experimental resolution. The statistical uncertainties in the data were propagated to the extracted poles using the bootstrap technique. We do not find support for a bound molecule. Based on a systematic analysis of the reaction amplitudes, we conclude instead that the interpretation of the $P_c(4312)^+$ peak as a virtual (unbound) state is more likely.

Acknowledgments.— We thank Tomasz Skwarnicki for discussions and useful comments on the manuscript. This work was supported by the U.S. Department of Energy under Grants No. DE-AC05-06OR23177 and No. DE-FG02-87ER40365, U.S. National Science Foundation Grant No. PHY-1415459, PAPIIT-DGAPA (UNAM, Mexico) under Grant No. IA101819, and CONACYT (Mexico) under Grants No. 251817, No. 619970 and No. A1-S-21389.

* cesar.fernandez@nucleares.unam.mx
† pillaus@jlab.org

[1] M. Gell-Mann, Phys.Lett. **8**, 214 (1964).
[2] G. Zweig, *An SU(3) model for strong interaction symmetry and its breaking*, Tech. Rep. CERN-TH-401 (CERN, Geneve, Switzerland, 1964).
[3] A. Esposito, A. Pilloni, and A. D. Polosa, Phys.Rept. **668**, 1 (2017), arXiv:1611.07920 [hep-ph].
[4] R. F. Lebed, R. E. Mitchell, and E. S. Swanson, Prog.Part.Nucl.Phys. **93**, 143 (2017), arXiv:1610.04528 [hep-ph].
[5] F.-K. Guo, C. Hanhart, U.-G. Meißner, Q. Wang, Q. Zhao, and B.-S. Zou, Rev.Mod.Phys. **90**, 015004 (2018), arXiv:1705.00141 [hep-ph].
[6] S. L. Olsen, T. Skwarnicki, and D. Zieminska, Rev.Mod.Phys. **90**, 015003 (2018), arXiv:1708.04012 [hep-ph].
[7] M. Karliner, J. L. Rosner, and T. Skwarnicki, Ann.Rev.Nucl.Part.Sci **68** (2018), 10.1146/annurev-nucl-101917-020902, arXiv:1711.10626 [hep-ph].
[8] A. Ali, L. Maiani, and A. Polosa, *Multiquark Hadrons* (Cambridge University Press, 2019).
[9] R. Aaij *et al.* (LHCb Collaboration), (2019), arXiv:1904.03947 [hep-ex].
[10] R. Aaij *et al.* (LHCb Collaboration), Phys.Rev.Lett. **115**, 072001 (2015), arXiv:1507.03414 [hep-ex].
[11] R. Aaij *et al.* (LHCb Collaboration), Phys.Rev.Lett. **117**, 082002 (2016), arXiv:1604.05708 [hep-ex].
[12] J.-J. Wu, R. Molina, E. Oset, and B. S. Zou, Phys.Rev.Lett. **105**, 232001 (2010), arXiv:1007.0573 [nucl-th].
[13] J.-J. Wu, R. Molina, E. Oset, and B. S. Zou, Phys.Rev. **C84**, 015202 (2011), arXiv:1011.2399 [nucl-th].
[14] W. L. Wang, F. Huang, Z. Y. Zhang, and B. S. Zou, Phys.Rev. **C84**, 015203 (2011), arXiv:1101.0453 [nucl-th].
[15] Z.-C. Yang, Z.-F. Sun, J. He, X. Liu, and S.-L. Zhu, Chin.Phys. **C36**, 6 (2012), arXiv:1105.2901 [hep-ph].
[16] C. W. Xiao, J. Nieves, and E. Oset, Phys.Rev. **D88**, 056012 (2013), arXiv:1304.5368 [hep-ph].
[17] Y. Yamaguchi, A. Giachino, A. Hosaka, E. Santopinto, S. Takeuchi, and M. Takizawa, Phys. Rev. **D96**, 114031 (2017), arXiv:1709.00819 [hep-ph].
[18] R. J. Eden and J. R. Taylor, Phys.Rev. **133**, B1575 (1964).
[19] H. W. Hammer and S. König, Phys.Lett. **B736**, 208 (2014), arXiv:1406.1359 [nucl-th].
[20] R. Zhu and C.-F. Qiao, Phys.Lett. **B756**, 259 (2016), arXiv:1510.08693 [hep-ph].
[21] L. Maiani, A. D. Polosa, and V. Riquer, Phys.Lett. **B749**, 289 (2015), arXiv:1507.04980 [hep-ph].
[22] S. H. Blitz and R. F. Lebed, Phys.Rev. **D91**, 094025 (2015), arXiv:1503.04802 [hep-ph].
[23] A. Esposito, A. Pilloni, and A. D. Polosa, Phys.Lett. **B758**, 292 (2016), arXiv:1603.07667 [hep-ph].
[24] R. Chen, X. Liu, Z.-F. Sun, and S.-L. Zhu, (2019), arXiv:1903.11013 [hep-ph].
[25] H.-X. Chen, W. Chen, and S.-L. Zhu, (2019), arXiv:1903.11001 [hep-ph].
[26] F.-K. Guo, H.-J. Jing, U.-G. Meißner, and S. Sakai, (2019), arXiv:1903.11503 [hep-ph].
[27] M.-Z. Liu, Y.-W. Pan, F.-Z. Peng, M. Sanchez Sanchez, L.-S. Geng, A. Hosaka, and M. Pavon Valderrama, (2019), arXiv:1903.11560 [hep-ph].
[28] H. Huang, J. He, and J. Ping, (2019), arXiv:1904.00221 [hep-ph].
[29] A. Ali and A. Ya. Parkhomenko, (2019), arXiv:1904.00446 [hep-ph].
[30] C.-J. Xiao, Y. Huang, Y.-B. Dong, L.-S. Geng, and D.-Y. Chen, (2019), arXiv:1904.00872 [hep-ph].
[31] Y. Shimizu, Y. Yamaguchi, and M. Harada, (2019), arXiv:1904.00587 [hep-ph].
[32] Z.-H. Guo and J. A. Oller, (2019), arXiv:1904.00851 [hep-ph].
[33] C. W. Xiao, J. Nieves, and E. Oset, (2019), arXiv:1904.01296 [hep-ph].
[34] W. R. Frazer and A. W. Hendry, Phys.Rev. **134**, B1307 (1964).
[35] S. Weinberg, Phys.Rev. **137**, B672 (1965).
[36] F. Aceti and E. Oset, Phys.Rev. **D86**, 014012 (2012), arXiv:1202.4607 [hep-ph].
[37] T. Sekihara, T. Hyodo, and D. Jido, PTEP **2015**, 063D04 (2015), arXiv:1411.2308 [hep-ph].
[38] Z.-H. Guo and J. A. Oller, Phys.Rev. **D93**, 096001 (2016), arXiv:1508.06400 [hep-ph].

[39] V. Baru, J. Haidenbauer, C. Hanhart, Yu. Kalashnikova, and A. E. Kudryavtsev, Phys.Lett. **B586**, 53 (2004), arXiv:hep-ph/0308129 [hep-ph].
[40] M. Tanabashi *et al.* (Particle Data Group Collaboration), Phys.Rev. **D98**, 030001 (2018).
[41] "Supplemental material," Also on http://www.indiana.edu/∼jpac/pc4312.php.
[42] A. Pilloni, C. Fernández-Ramírez, A. Jackura, V. Mathieu, M. Mikhasenko, J. Nys, and A. P. Szczepaniak (JPAC Collaboration), Phys.Lett. **B772**, 200 (2017), arXiv:1612.06490 [hep-ph].
[43] E. Braaten and M. Lu, Phys.Rev. **D76**, 094028 (2007), arXiv:0709.2697 [hep-ph].
[44] F. James and M. Roos, Comput.Phys.Commun. **10**, 343 (1975).
[45] S. S. Wilks, Annals Math.Statist. **9**, 60 (1938).
[46] W. H. Press, S. A. Teukolsky, W. T. Vetterling, and B. P. Flannery, *Numerical Recipes 3rd Edition: The Art of Scientific Computing*, 3rd ed. (Cambridge University Press, New York, NY, USA, 2007).
[47] B. Efron and R. Tibshirani, *An Introduction to the Bootstrap*, Chapman & Hall/CRC Monographs on Statistics & Applied Probability (Taylor & Francis, 1994).
[48] A. Rodas *et al.* (JPAC Collaboration), Phys.Rev.Lett. **122**, 042002 (2019), arXiv:1810.04171 [hep-ph].

SUPPLEMENTAL MATERIAL

- The animations of the pole motion are available in GIF format on http://www.indiana.edu/~jpac/pc4312.php.
- We write here the explicit formula for the amplitudes described in the text. We use isospin to relate the $\Sigma_c^+ \bar{D}^0$ and the $\Sigma_c^{++} D^-$ channels.

$$\frac{dN}{d\sqrt{s}} = \rho(s)\left[|F(s)|^2 + B(s)\right],$$
$$F(s) = P_1(s) T_{11}(s),$$

$$T(s) = \begin{pmatrix} m_{11} - c_{11}s - i\sqrt{s-s_1} & m_{12} & \lambda m_{12} \\ m_{12} & m_{22} - c_{22}s - i\sqrt{s-s_2} & \lambda m_{23} \\ \lambda m_{12} & \lambda m_{23} & \lambda\left(m_{22} - c_{22}s - i\sqrt{s-s_3}\right) \end{pmatrix}^{-1},$$

with $s_1 = (m_\psi + m_p)^2$, $s_3 = \left(m_{\Sigma_c^+} + m_{\bar{D}^0}\right)^2$, $s_3 = \left(m_{\Sigma_c^{++}} + m_{D^-}\right)^2$.

TABLE I. Summary of fit results for the two cases described in the text. Appropriate powers of GeV units are understood. The function $P_1(s)$ is parameterized as $p_0 + p_1 s$ and $B(s)$ as $b_0 + b_1 s$. In each case the χ^2/dof corresponds to the best fit obtained. The first column of parameters is obtained from the best fit, and should be used to reproduce the plots. The second column reports the mean value and uncertainty of the parameters from bootstrap. The phase space factor for the decay $\Lambda_b^0 \to J/\psi\, p\, K^-$ appearing in Eq. (1) is given by $\rho(s) = m_{\Lambda_b} p\, q$ with $p = \lambda^{1/2}(s, m_{\Lambda_b}^2, m_K^2)/2m_{\Lambda_b}$, $q = \lambda^{1/2}(s, m_p^2, m_\psi^2)/2\sqrt{s}$, and $\lambda(x,y,z) = x^2 + y^2 + z^2 - 2xy - 2xz - 2yz$ is the Källén function.

	Case A		Case B		3-channel	
χ^2/dof	$48.1/(66-7) = 0.82$		$43.0/(66-9) = 0.75$		$45.5/(66-8) = 0.78$	
	best fit	bootstrap	best fit	bootstrap	best fit	bootstrap
b_0	402.95	446 ± 73	0.74	6.1 ± 6.0	121.56	123.1 ± 1.4
b_1	-15.00	-17.4 ± 4.1	7.22	6.93 ± 0.36	0.63	0.52 ± 0.14
p_0	423.16	437 ± 16	85.06	92.6 ± 8.8	422.72	422.52 ± 0.38
p_1	-23.53	-24.28 ± 0.81	-5.30	-5.70 ± 0.47	-23.41	-23.409 ± 0.040
m_{11}	2.60	2.65 ± 0.28	151.29	151.35 ± 0.23	2.83	2.82 ± 0.19
m_{22}	0.22	0.223 ± 0.078	38.81	39.12 ± 0.28	-4.27	-4.259 ± 0.042
m_{12}	0.85	0.86 ± 0.11	1.03	1.035 ± 0.062	0.64	0.646 ± 0.057
m_{23}	0	0	0	0	4.38	4.385 ± 0.022
c_{11}	0	0	8.00	8.007 ± 0.015	0	0
c_{22}	0	0	-2.06	2.081 ± 0.016	0	0
c_{12}	0	0	0	0	0	0
λ	0	0	0	0	1	1

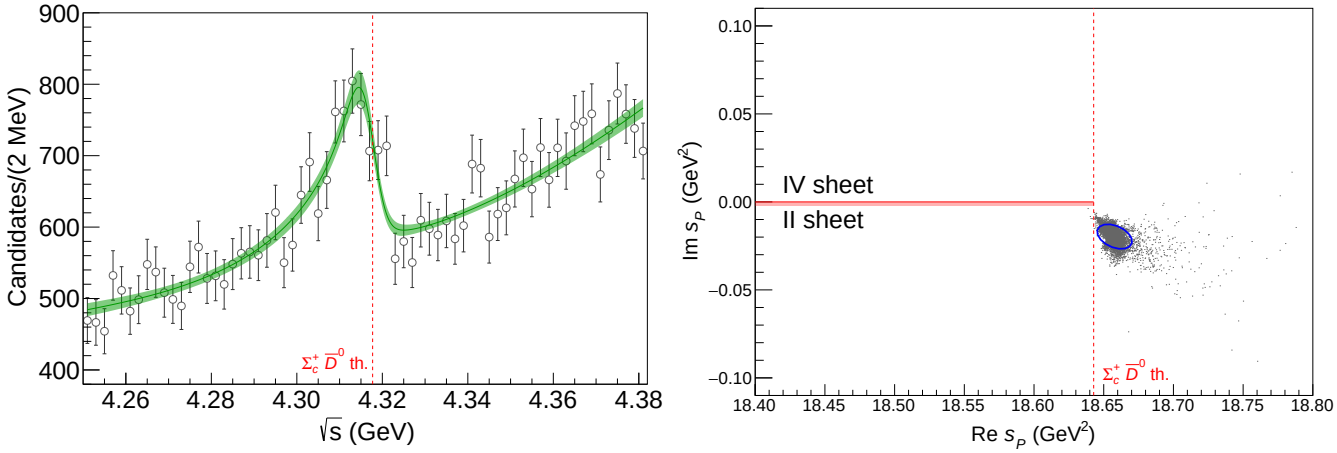

FIG. 4. Fit to the $\cos\theta_{P_c}$-weighted $J/\psi\, p$ mass distribution (left) and pole positions (right) for the K-matrix case. Notation is the same as in Figs. 1 and 2. The poles are obtained from the 10^4 bootstrap fits and lie on the II and IV Riemann sheets (which are continuously connected above the $\Sigma_c^+ \bar{D}^0$ threshold).

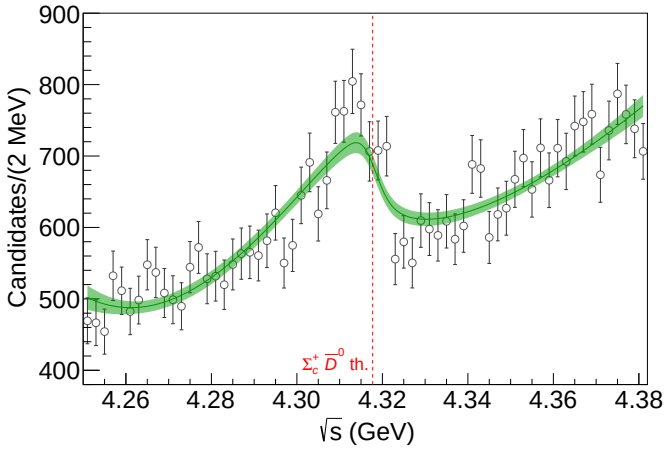

FIG. 5. Fit to the $\cos\theta_{P_c}$-weighted $J/\psi\, p$ mass distribution for the Flatté case. Notation is as in Fig. 1. This parameterization does not generate a pole in the region of interest.